THE JOURNAL OF BIOLOGICAL CHEMISTRY VOL. 290, NO. 43, pp. 25851–25862, October 23, 2015

Neuronal ClC-3 Splice Variants Differ in Subcellular Localizations, but Mediate Identical Transport Functions*

Received for publication, May 29, 2015, and in revised form, August 26, 2015 Published, JBC Papers in Press, September 4, 2015, DOI 10.1074/jbc.M115.668186

Raul E. Guzman[1], **Erick Miranda-Laferte**[2], **Arne Franzen, and Christoph Fahlke**[3]

From the Institute of Complex Systems, Zelluläre Biophysik (ICS-4), Forschungszentrum Jülich, 52425 Jülich, Germany

Background: Alternative splicing can result in proteins with distinct subcellular distributions and functions.
Results: Three ClC-3 splice variants are expressed in the mammalian brain with different subcellular localizations, but identical transport properties.
Conclusion: Differences in the subcellular localization of ClC-3 splice variants suggest diverse cellular functions.
Significance: The existence of multiple splice variants needs to be considered when studying cellular functions of ClC-3.

ClC-3 is a member of the CLC family of anion channels and transporters, for which multiple functional properties and subcellular localizations have been reported. Since alternative splicing often results in proteins with diverse properties, we investigated to what extent alternative splicing might influence subcellular targeting and function of ClC-3. We identified three alternatively spliced ClC-3 isoforms, ClC-3a, ClC-3b, and ClC-3c, in mouse brain, with ClC-3c being the predominant splice variant. Whereas ClC-3a and ClC-3b are present in late endosomes/lysosomes, ClC-3c is targeted to recycling endosomes via a novel N-terminal isoleucine-proline (IP) motif. Surface membrane insertion of a fraction of ClC-3c transporters permitted electrophysiological characterization of this splice variant through whole-cell patch clamping on transfected mammalian cells. In contrast, neutralization of the N-terminal dileucine-like motifs was required for functional analysis of ClC-3a and ClC-3b. Heterologous expression of ClC-3a or ClC-3b carrying mutations in N-terminal dileucine motifs as well as WTClC-3c in HEK293T cells resulted in outwardly rectifying Cl^- currents with significant capacitive current components. We conclude that alternative splicing of *Clcn3* results in proteins with different subcellular localizations, but leaves the transport function of the proteins unaffected.

ClC-3 belongs to the sub-branch of the CLC family of anion channels and transporters that resides primarily in intracellular organelles. Its functional relevance in the central nervous system is illustrated by $Clcn3^{-/-}$ knock-out animal models (1–3) that exhibit pronounced hippocampal and retinal degeneration. Changes in synaptic transmission in these animals suggest that ClC-3 is present in synaptic vesicles and contributes to the regulation of neurotransmitter accumulation and release from the presynaptic nerve terminal (2, 4, 5).

However, besides experimental data that supports localization of ClC-3 in synaptic vesicles or lysosomes (2–8), there are also results that argue in favor of surface membrane localization of this protein (9, 10). Moreover, multiple functional properties have been reported for ClC-3. Our group expressed mutant ClC-3 after removal of an N-terminal dileucine motif and observed outwardly rectifying anion-proton exchange current that resemble currents mediated by ClC-4 and ClC-5 (11–15). A characteristic property of ClC-3 was the occurrence of prominent capacitive currents, which indicate a large percentage of transporters mediating incomplete transport cycles (12, 16). Other groups assigned a postsynaptic Ca/CaMK-regulated anion channel in hippocampal neurons to ClC-3 and hypothesized that ClC-3 might regulate neuronal excitability as anion channels by modifying the postsynaptic membrane potential and/or length constant (9, 10, 17).

A potential reason for such functional differences between native and heterologously expressed proteins might be the existence of alternatively spliced ClC-3 variants with distinct subcellular localizations and transport functions. So far, five splice variants of *Clcn-3* have been identified; ClC-3a, ClC-3b, ClC-3c, ClC-3d, and ClC-3e, and partially characterized (18–20). We decided to clone all ClC-3 splice variants from mouse brain and to compare their functions and subcellular distributions. We found three splice variants that differ in the N-terminal domain and exhibit identical transport function, but different subcellular distributions.

Experimental Procedures

Cloning and Expression Profile of ClC-3a, ClC-3b, and ClC-3c—To clone the complete coding regions of ClC-3a, ClC-3b, and ClC-3c, cDNAs were amplified from mouse brain using the SuperScript™ one step RT-PCR system with platinum Taq (Invitrogen, Carlsbad, CA). We used primers that were specific to the different 5′ coding region together with a common reverse primer hybridizing to the 3′-end. After assembly of amplified bands into the pRSETB vector (Invitrogen) variants were identified by sequencing.

The tissue distribution of the different ClC-3 mRNAs was determined by RT-PCR. After isolation of total RNA from brain, heart, pancreas, kidney, liver, lung, retina, olfactory bulb, and spinal cord from 2-month-old mice and from hippocampi

* The authors declare that they have no conflicts of interest with the contents of this article.
[1] To whom correspondence may be addressed. E-mail: r.guzman@fz-juelich.de.
[2] Present address: Physiologisches Institut, Universität Würzburg, 97070 Würzburg, Germany.
[3] To whom correspondence may be addressed: Institute of Complex Systems, Zelluläre Biophysik (ICS-4), Forschungszentrum Jülich, 52425 Jülich, Germany. E-mail: c.fahlke@fz-juelich.de.

from 2, 13, 30, 60, or 120 days old mice RT-PCR was performed with the following primers: for ClC-3a and ClC-3b 5′-CGCCCAGCTTGCTATGCCTCTGAG-3′ (forward), ClC-3c 5′-ATGGATGCTTCTTCTGATCC-3′ (forward) and a common antisense primer 5′-AGCTAGTGCCCCTGATGCCAGTC-3′ (reverse). Three PCR products with the predicted size of 324 bp/ClC-3a, 500 bp/ClC-3b, and 379 bp/ClC-3c were obtained. To identify ClC-3e (ClC-3d or ClC-3f), 5′-TGCCCTCAGAAGAGACCTGACTATTGC-3′ (forward) and 5′-AACGAACTTCCTCTTCTGTCTCCTCTCTG-3′ (reverse) primers were applied. These primers recognize sequences in the 3′-coding region of *Clcn3* and generates RT-PCR products with expected sizes of 485 bp and 409 bp corresponding to the ClC-3 with the long and short C termini, respectively.

PCR products were separated by gel electrophoresis and quantified using ImageJ 1.44p software (National Institutes of Health, Bethesda, MD) (21). To account for age-dependent changes in cell number or size these values were normalized to mRNA levels of glyceraldehyde-3-phosphate dehydrogenase (GAPDH). GAPDH mRNA levels were determined using 5′-CAGTATGACTCCACTCACGGCAAATTC-3′ as forward primer and 5′-CACAGTCTTCTGGGTGGCAGTGATG-3′ as reverse primer, generating a PCR product with an expected size of 423 bp.

Heterologous Expression—cDNAs encoding full-length mouse ClC-3a, ClC-3b, or ClC-3c (GenBank^{TM} Accession Number NM_007711.3, NM_173873.1, NM_173876.3) were fused in-frame to the 5′-end of the coding sequences of enhanced green or monomeric red fluorescence protein (eGFP or mRFP) and cloned into FsY1.1 G.W. or p156rrL vectors (were kindly provided by Dr. M. Filippov, Nizhny Novgorod, Russia, and Dr. D. Bruns, Homburg, Germany). For each construct, two independent recombinants from the same transformation were examined and shown to exhibit indistinguishable functional properties.

ClC-3 splice variants were transiently expressed in HEK293T or MDCK II cells alone or in combination with fluorescent markers such as LAMP1 (which was a gift from Walther Mothes (Addgene plasmid 1817) (22), RAB7, RAB11 (a gift from Richard Pagano (Addgene plasmid 12605) (23), TfR (a gift from Gary Banker (Addgene plasmid 45060) (24), or the membrane marker farnesylated eGFP (provided by Dr. M. Filippov, Nizhny Novgorod, Russia) and examined typically 24 h or 36 h after transfection of 2 to 5 μg of cDNA using Lipofectamine 2000 (Invitrogen) or calcium phosphate transfection methods (25).

Electrophysiology—Standard whole-cell patch clamp recordings were performed using an EPC-10 amplifier, software controlled by PatchMaster (HEKA) (11). Borosilicate pipettes (Harvard Apparatus) were pulled with resistances of 0.9–2 MΩ. We only recorded from cells with series resistances below 4.5 MΩ. More than 80% of the series resistance was routinely compensated, resulting in a voltage error of less than 5 mV. P/4 leak subtraction with a baseline potential of −30 mV was used to cancel linear capacitances (26). Currents were low-pass filtered at 2.9 kHz and digitalized with a sampling rate of 100 kHz. The standard external and internal recording solutions contained (in mM) 160 NaCl, 15 HEPES, 4 K-gluconate, 2 $CaCl_2$, 1 $MgCl_2$, pH 7.4 (bath solution), or 105 NaCl, 15 HEPES, 5 $MgCl_2$, 5 EGTA; pH 7.4 (pipette solution).

Confocal Imaging—Images were acquired 24–36 h after transfection with a Leica TCS SP5 II inverted microscope (Manheim, Germany) using a 63× oil immersion objective from living cells in PBS containing Ca^{2+} and Mg^{2+} (GIBCO) at room temperature (22–24 °C). EGPF and YFP (enhance green and yellow fluorescence proteins) fluorophores were excited with a 488-nm Argon laser and mRFP (monomeric red fluorescence protein) with a 594-nm He-Ne laser. Emission signals were detected after filtering with at 500–550 nm, 520–560 nm, or 600–650 nm bandpass filters. To determine the fraction of ClC-3b mutants inserted into the plasma membrane (Fig. 4*H*) we co-expressed farnesylated eGFP as surface membrane marker together with ClC-3b$_{S3/S2}$ ClC-3b$_{S3/S1}$ orClC-3b$_{S3/S2/S1}$ as mRFP fusion proteins. Surface membrane insertion was then quantified in confocal images as mRFP fluorescence intensity overlapping with eGFP fluorescence. For all mutants we used similar microscope settings in these experiments. Images were analyzed and assembled for publications in ImageJ 1.44p software (National Institutes of Health) (21).

Protein Purification and Pull-down Experiments—Glutathione *S*-transferase (GST)-fusion constructs (GST-NT ClC-3b and GST-NT ClC-3b$_{S3/S2/S1}$) were generated by amplifying DNA fragments encoding amino acids 1–125aa of ClC-3b and ClC-3b$_{S3/S2/S1}$ using PCR. These fragments were then cloned into the PGEX-6P1 (GE Healthcare, Freiburg, Germany) vector and verified by sequencing. GST-fusion proteins (GST-NT ClC-3b, GST-NT ClC-3b$_{S3/S2/S1}$, and GST alone) were expressed in *Escherichia coli* (BL21) for 4–5 h at 30 °C after induction with isopropyl β-D-1-thiogalactopyranoside (IPTG) and purified using affinity and size-exclusion chromatography as described previously (27, 28). For pull-down experiments brain lysates were produced by homogenization of brain tissue from C57Bl/6 mice and two consecutive rounds of centrifugation. 1 ml of the resulting mouse brain lysate were incubated with 5 μg of GST-fusion protein (GST-NT ClC-3b, GST-NT ClC-3b$_{S3/S2/S1}$, or GST alone) bound to glutathione-Sepharose (GE Healthcare, Freiburg, Germany) for 4 h at 4 °C under constant agitation. After 5–6 times washing with HBS containing 0.1% (*w*/*v*) Triton X-100 proteins were eluted with SDS loading buffer, separated by SDS-PAGE and analyzed by immunoblotting with antibodies against clathrin (BD Biosciences, Heidelberg, Germany).

Data Analysis—Data analysis was performed using a combination of FitMaster (HEKA), Origin (OriginLab), SigmaPlot (Systat Software), and Excel (Microsoft) software. All data are presented as mean ± S.E.

Results

Cloning and Expression Profiles of Mouse ClC-3 Splice Variants—Four alternatively spliced ClC-3 isoforms, ClC-3a, ClC-3b, ClC-3c, and ClC-3e (GenBank^{TM} Accession Number NM_007711.3, NM_173873.1, NM_173876.3, NM_173874.1), can be found in protein sequence data bases. ClC-3a is the shortest ClC-3 splice variant with 760 amino acids. Its expression results from a start codon downstream of the first AUG of other variants (Fig. 1*A*) (Clcn3 chloride channel 3 (Mus muscu-

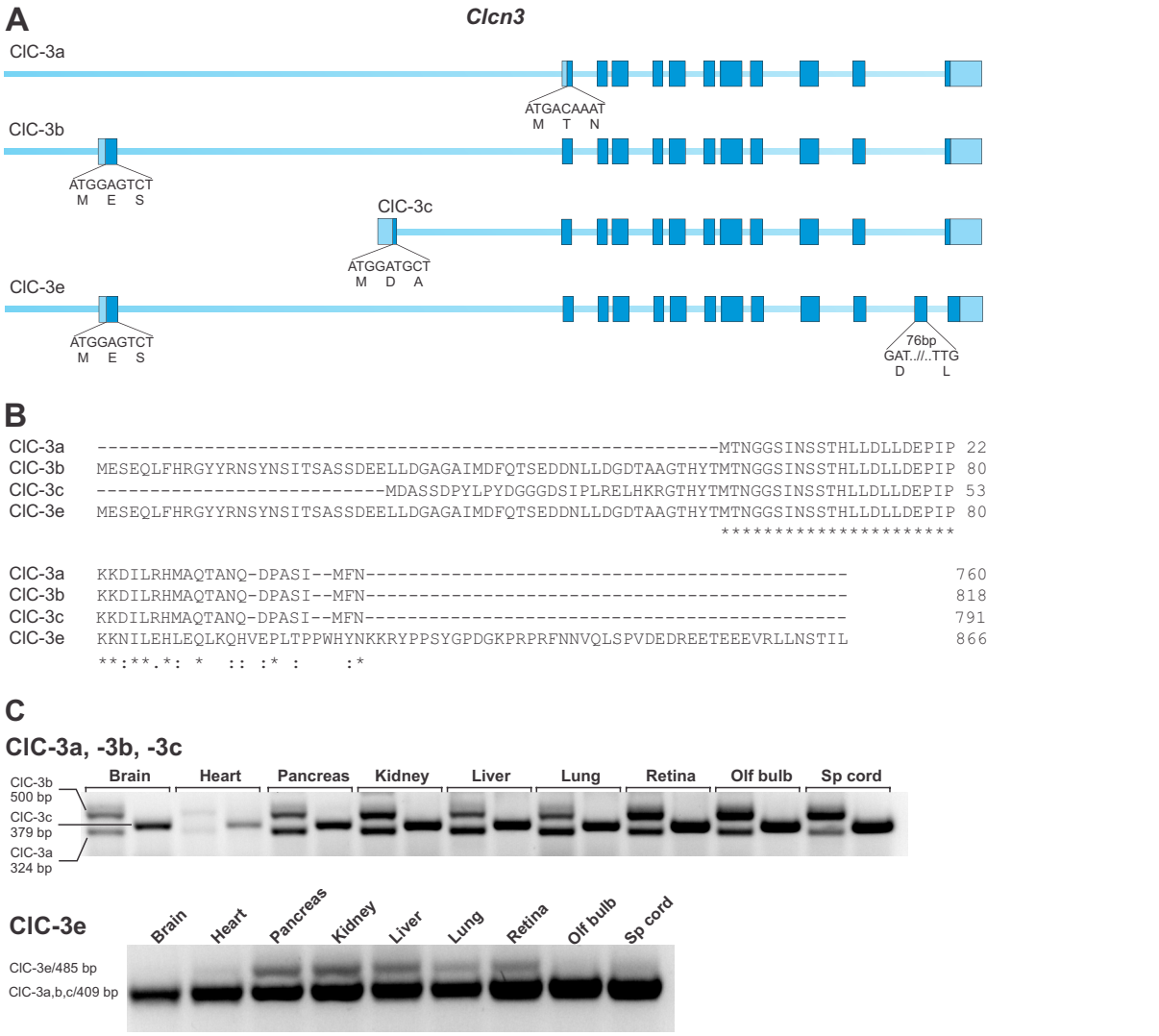

FIGURE 1. **Multiple ClC-3 splice variants in mouse tissue.** *A*, genomic organization of the mouse *Clcn3* gene. *Solid bars* represent coding regions (exons; *blue*) non-translated regions (*light blue*), and introns (*solid lines*, *light blue*). The genomic sequence for the first 9 nucleotides including the start codon and the corresponding translated amino acids are given for each splice variant. *B*, sequence alignment of N- and C-terminal regions of the predicted ClC-3 splice variants. Conserved residues are denoted with *. *C*, tissue distribution of ClC-3 splice variants were examined by RT-PCR; expected PCR product size were: ClC-3a 324 bp, ClC-3b 500 bp, ClC-3c 379 bp, and ClC-3e 485 bp.

lus (house mouse)), NCBI accession number 12725). ClC-3b, sometimes also denoted as ClC-3A (18, 19), and ClC-3c possess an alternative in-frame exon in the 5′ coding region, resulting in N-terminal domains of different lengths (Fig. 1*A*) (Clcn3 chloride channel 3 (Mus musculus (house mouse)), NCBI accession number 12725) and with 58 (ClC-3b) or 31 (ClC-3c) additional amino acids residues as compared with ClC-3a (Fig. 1*B*). For ClC-3e, also denoted as ClC-3B (18, 19), insertion of an alternate exon (76 bp) in the 3′ coding region generates a frameshift that results in a ClC-3 splice variant that differs from ClC-3b by additional amino acids in the C-terminal region (Fig. 1*B*). Further splice variants harboring the N-terminal domains of ClC-3a or ClC-3c combined with the C terminus of ClC-3e were denoted as ClC-3d (20) and ClC-3f. We used RT-PCR to determine the tissue distribution of ClC-3 splice variants taking advantage of the distinct 5′ and 3′ coding region of *ClCn3*. Splice variant-specific PCR products (Fig. 1*C*, ClC-3a; 324 bp, ClC-3b; 500 bp, ClC-3c; 379 bp) demonstrate ubiquitous expression of ClC-3a, ClC-3b and ClC-3c mRNA. Although this approach does not allow distinction between ClC-3d, ClC-3e, and ClC-3f (485bp), it permits demonstration that ClC-3 splice variants with long C terminus are only expressed in pancreas, kidney, liver, lung, and retina, but not in any other region of the central nervous system (CNS). *Clcn3*$^{-/-}$ animals exhibit a severe neurological phenotype (1–3), and we therefore decided to focus on alternative splice variants that are expressed in the central nervous system, ClC-3a, ClC-3b, and ClC-3c.

Hippocampal degeneration in *Clcn3*$^{-/-}$ mice starts about 2 weeks after birth (1–3). We reasoned that developmental changes in splice variant expression might contribute to this age dependence. Since there are no splice variant-specific antibodies available that distinguish between ClC-3a, ClC-3b, and ClC-3c, quantification of protein expression levels by Western blot analysis is not possible. We therefore examined mRNA profiles in hippocampal tissue from 2, 13, 30, 60, or 120 days old

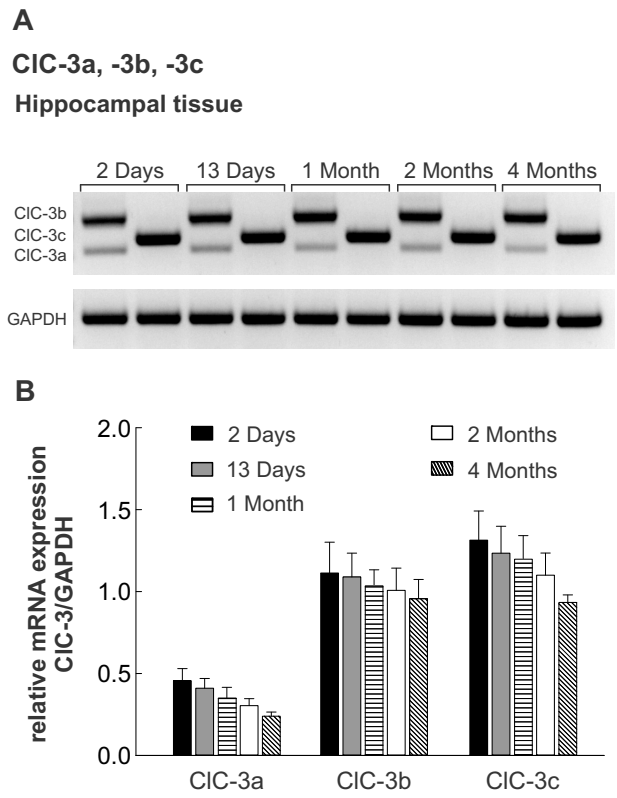

FIGURE 2. **Developmental expression of the ClC-3 splice variants in hippocampal tissue.** *A*, representative RT PCR experiment of ClC-3 variants extracted from mouse hippocampus at different ages. *B*, age dependence of ClC-3a, ClC-3b, and ClC-3c mRNA levels normalized to the respective GAPDH mRNA levels and given as means ± S.E. from three independent experiments.

mice (Fig. 2, *A* and *B*). We did not observe significant age-dependent changes in the mRNA levels for any ClC-3 splice variants relative to the amount of GAPDH mRNA (Fig. 2, *A* and *B*). Comparison of mRNA levels demonstrated relatively low levels of ClC-3a mRNA and much stronger transcription of ClC-3b and ClC-3c mRNA at all tested ages. These data show that mRNA levels of ClC-3a, ClC-3b and ClC-3c remain unchanged at juvenile, early adult and adult ages and that ClC-3b and ClC-3c are the predominant ClC-3 splice variant in hippocampal neurons.

ClC-3 Splice Variants Exhibit Different Subcellular Localizations—Differences in primary structure might result in altered transport functions and/or subcellular distribution of ClC-3 splice variants. We therefore studied biophysical properties and subcellular localization of ClC-3b and ClC-3c and compared them with the well characterized short isoform ClC-3a (16). Whole-cell recordings of HEK293T cells heterologously expressing WT ClC-3a or WT ClC-3b yielded ionic currents undistinguishable from non-transfected cells (Fig. 3*A*). In contrast, we were able to record ClC-3-specific currents from cells expressing WT ClC-3c. At positive potentials these cells display outwardly rectifying Cl^- currents with amplitudes up to 1.5 nA at +175 mV, whereas no measurable currents could be observed at negative potentials. Upon depolarizing voltage steps, there are large peaks at the beginning of the applied voltage steps that resemble the gating charge movements of ClC-5 (29) and ClC-3_{13-19A} (a ClC-3a mutant in which an N-terminal dileucine motif had been mutated (8, 16)) (Fig. 3*A*).

The differences in functional expression are due to separate subcellular targeting of the distinct splice variants (Fig. 3*B*). Upon expression of ClC-3a or of ClC-3b transfected cells exhibit large vesicular structures that co-localize with the lysosomal marker LAMP1 and therefore likely originate from lysosomal compartments. ClC-3c exhibited a different intracellular localization, which results in staining of the surface membrane and of intracellular vesicular compartments that do not contain LAMP1 (Fig. 3*B*). Complementary experiments revealed identical subcellular distribution of ClC-3 splice variants in MDCK cells as in HEK293T cells (data not shown).

The N Terminus of ClC-3b Contains Three Potential Dileucine Motifs—Alternative splicing in the N-terminal region might not only modify the subcellular distribution, but also the function of ClC-3, as reported for many other proteins (30–33). We therefore searched for the signals that are responsible for the intracellular localization of ClC-3b and whose deletion might allow membrane surface insertion and electrophysiological characterization. For ClC-3a removal of a dileucine motif sequence (LLDLLDE (S1) Fig. 4*A*) allows surface membrane insertion and functional analysis of the protein (8, 16, 34). ClC-3b contains the same sequence motif, however, its removal did not result in surface membrane insertion (data not shown). We therefore screened the N-terminal region of ClC-3b for additional dileucine motifs (Fig. 4*A*). We found two such sequences, ^{42}EDDNLL^{47} (S2) and ^{26}EELL^{29} (S3), and generated mutant constructs in which either two of the three motifs (ClC-$3b_{S3/S2}$ and ClC-$3_{S3/S1}$) or all dileucine motifs (ClC-$3b_{S3/S2/S1}$) were substituted by alanine. Removal of only two dileucine motifs (ClC-$3b_{S3/S2}$ and ClC-$3_{S3/S1}$) resulted in surface membrane localization of a fraction of the expressed proteins. However, there was still some fluorescence staining of intracellular compartments and large LAMP1-positive vesicular structures. ClC-$3b_{S3/S2/S1}$, in which all three dileucine motifs were removed, inserted predominantly into the surface membrane so that the large vesicular structures induced by ClC-$3b_{S3/S2}$ and ClC-$3_{S3/S1}$ were absent in cell expressing this mutant protein (Fig. 4*B*).

To investigate interactions of the dileucine motifs with components of the endocytotic machinery using a pull-down strategy, we generated recombinant GST fusion proteins of N-terminal regions of ClC-3b wild type and ClC-$3b_{S3/S2/S1}$. After purification N-terminal fusion proteins were incubated with equal amount of mice brain lysate, and potential binding partners were analyzed by immunoblotting with antibodies to clathrin. Whereas GST-NT ClC-3b exhibits strong binding to clathrin (Fig. 4*C*), this interaction was markedly reduced for mutant GST-NT ClC-$3b_{S3/S2/S1}$ (Fig. 4*C*). These results suggest that the removal of ClC-3b dileucine motifs results in reduced internalization of the mutant protein (8). Alternatively, these mutations might enhance ClC-3b insertion into the plasma membrane via impaired recognition of mutant sorting motifs by adaptor proteins in the trans-Golgi network or in endosomal compartments (35).

The altered localization of mutant ClC-3b permits the electrophysiological characterization of this splice variant. The existence of various ClC-3b mutants with different dileucine motifs also provides the possibility to test whether mutations

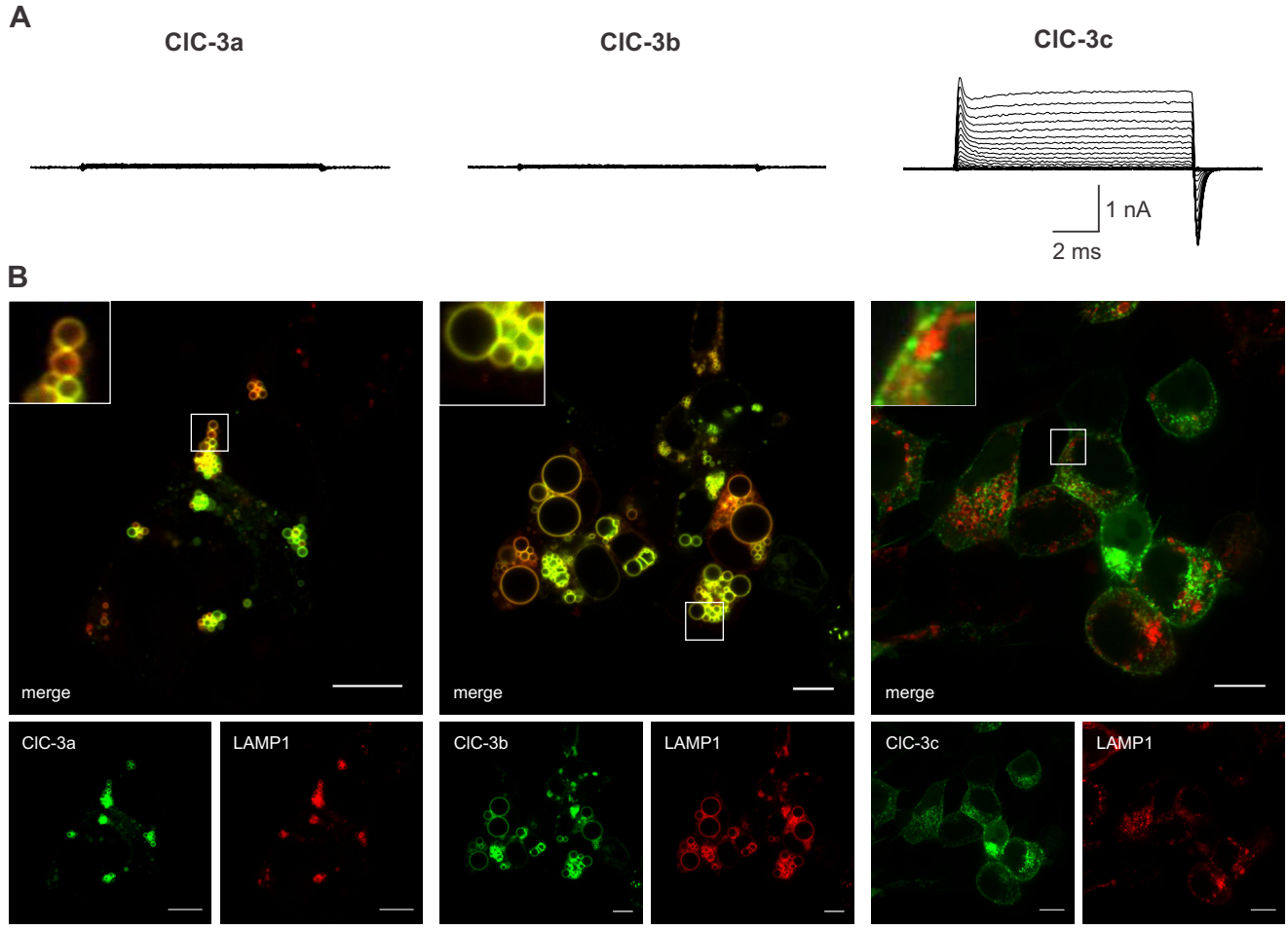

FIGURE 3. **Subcellular localization and whole-cell currents of neuronal ClC-3 splice variants.** *A,* representative whole-cell recordings of HEK293T cells heterologously expressing ClC-3a, ClC-3b, or ClC-3c. *B,* confocal images of cells co-transfected with either ClC-3a, ClC-3b, or ClC-3c (in *green*) and a fluorescent fusion protein of the lysosomal marker protein LAMP-1 (in *red*). Regions where both proteins overlap are shown as *orange*. The scale bar represents 10 μm. *Insets* show magnifications of the images illustrating the subcellular localization for ClC-3 proteins.

within the internalization motifs change functional properties. Mutant ClC-3b proteins with or without one dileucine motif expressed at sufficient amounts in the surface membrane to account for measurable outwardly rectifying Cl^- currents (Fig. 4, *D* and *E*). In all cases, we observed time and voltage-dependent currents that resemble ClC-$3a_{S1}$ (16). Expression of ClC-$3b_{S3/S2,}$ ClC-$3_{S3/S1,}$ or ClC-$3b_{S3/S2/S1}$ resulted in voltage-dependent outwardly rectifying currents at potentials positive to +35 mV, without inward currents at negative voltages (Fig. 4, *D* and *E*). Depolarizing voltage steps elicited a capacitive current followed by ionic current that slightly increased with time. Stepping back to the holding potential resulted in a capacitive current with identical amplitude as upon membrane depolarization. For CLC exchangers, a plot of the time integral of these capacitive currents, the "gating charge movement," *versus* the preceding voltage step provides the voltage dependence of activation (12, 16, 29, 36). Such analysis did not reveal any marked differences between the three mutants (Fig. 4*F*). For ClC-3, ClC-4, and ClC-5, such capacitive currents have been shown to originate from transporters that only perform incomplete transport cycles (12, 16), and the charge movement upon voltage steps thus provides a measure of transport-incompetent transporters. On the other hand, ionic currents are proportional to Cl^--H^+ exchange rates. Plotting gating charges *versus* ionic currents at the same voltage provides a value proportional to the transport competence of the different constructs (Fig. 4*G*). We observed identical slopes for ClC-$3b_{S3/S2}$, ClC-$3b_{S3/S1}$, and ClC-$3b_{S3/S2/S1}$.

The different macroscopic current amplitudes of cells expressing ClC-$3b_{S3/S2}$, ClC-$3b_{S3/S1}$, and ClC-$3b_{S3/S2/S1}$ are likely due to separate protein densities in the surface membrane (Fig. 4, *A* and *B*), but could be also affected by variation in individual transport rates. To distinguish between these two explanations we co-expressed mutant ClC-3b fusion proteins with farnesylated eGFP as surface membrane marker and calculated surface insertion probabilities as ratio of the mRFP fluorescence intensity in regions overlapping with farnesylated eGFP by whole-cell fluorescence in confocal images. A plot of mean macroscopic current amplitudes from cells expressing ClC-$3b_{S3/S2}$, ClC-$3b_{S3/S1}$, or ClC-$3b_{S3/S2/S1}$ against these values revealed a linear relationship (Fig. 4*H*), as expected for sole differences in trafficking and identical transport rates of the mutant transporters. We conclude that dileucine motifs in the N terminus exclusively affect trafficking, but not the transport activity of ClC-3b.

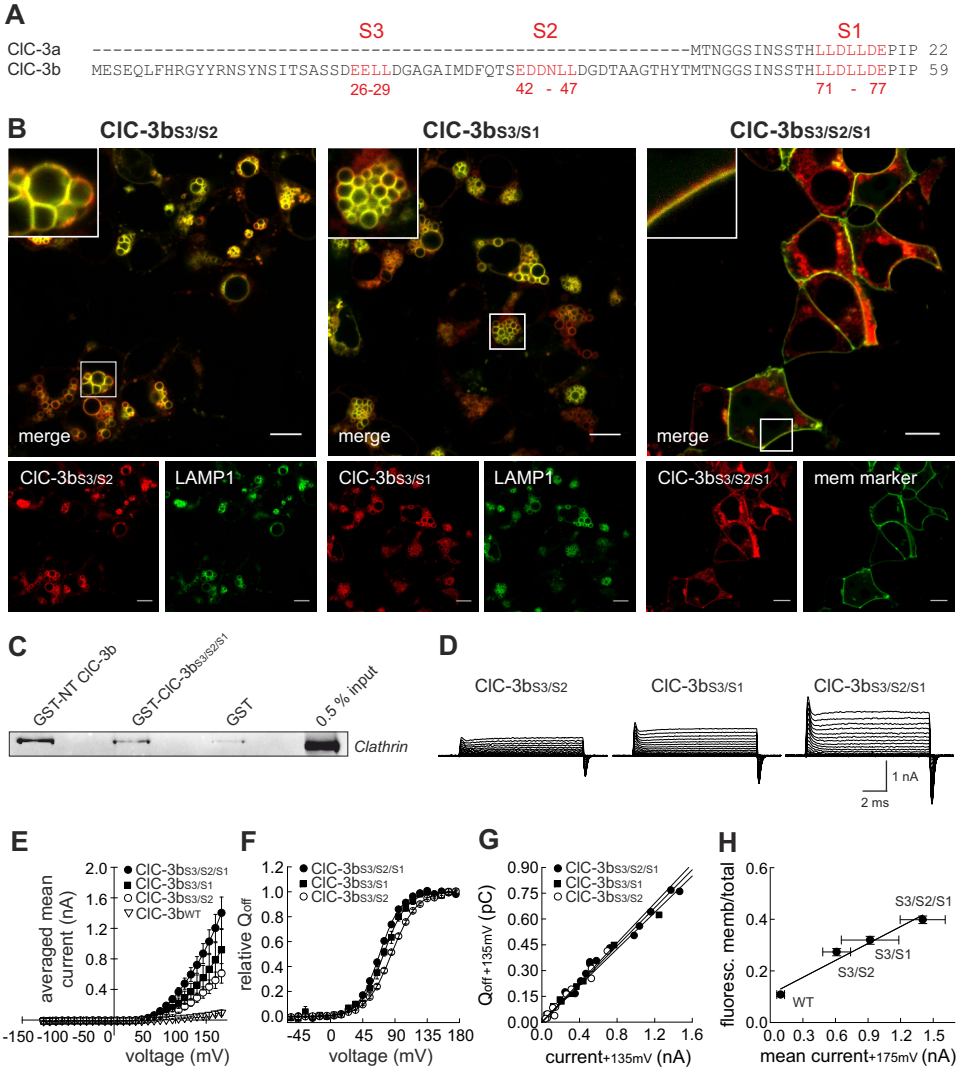

FIGURE 4. **ClC-3b contains multiple dileucine motifs in its N-terminal region.** *A,* sequence alignment of N-terminal regions of ClC-3a and ClC-3b. Sequences highlighted in *red* represent potential dileucine motifs; ^{71}LLDLLDE^{77} (S1), ^{42}EDDNLL^{47} (S2), and ^{26}EELL^{29} (S3). *B,* confocal images of cells co-transfected with mutant ClC-3b and either the lysosomal marker protein LAMP1 or the membrane marker eGFP-mem. The scale bar represents 10 μm. *C,* Western blot analyses from GST pull-down assay from mouse brain lysates with GST-NT ClC-3b or GST-NT ClC-3b$_{S3/S2/S1}$ or GST alone. *D,* representative whole-cell recording from cell expressing mutant ClC-3b. *E,* voltage dependence of mean current amplitudes for cells expressing WT or mutant ClC-3b obtained from recordings as shown in (*A*). Values are given as means ± S.E., WT ClC-3b (n = 4), ClC-3b$_{S3/S2}$ (n = 16), ClC-3$_{S3/S1}$ (n = 8), ClC-3b$_{S3/S2/S1}$ (n = 5). *F,* voltage dependence of the apparent gating charge movements for mutant ClC-3b constructs obtained from integrating the area under the nonlinear capacitive currents at the end of the voltage steps. *Lines* represent nonlinear fits to the data with standard Boltzmann function *G,* plot of current amplitudes of individual cells against the corresponding off-gating charge Q_{off} for ClC-3b$_{S3/S2}$, ClC-3$_{S3/S1}$, ClC-3b$_{S3/S2/S1}$ (n = 8–16). *Lines* represent linear fits with zero origin to the data. *H,* plot of the mean current amplitudes at +175 mV *versus* the relative surface membrane insertion probability for WT ClC-3b (n = 4 whole-cell recordings/25 confocal images), ClC-3b$_{S3/S2}$ (n = 16/55), ClC-3b$_{S3/S1}$ (n = 8/52) and ClC-3b$_{S3/S2/S1}$ (n = 5/64). Pearson correlation analyses reveal linear correlation between these two parameters (*Pearson coefficient* = 0.979; p = 0.02), and the *straight line* depicts a linear fit to these data.

Biophysical Properties of ClC-3 Splice Variants—Fig. 5 summarizes the electrophysiological analysis of the three variants, ClC-3a$_{S1}$, ClC-3b$_{S3/S2/S1}$, and ClC-3c. Each of the three ClC-3 proteins mediates outwardly rectifying currents (Fig. 5, *A* and *B*) with identical properties. In all cases, we observed large capacitive currents upon depolarization and subsequent repolarization to the holding potential. We quantified the voltage dependence of ClC-3a$_{S1}$, ClC-3b$_{S3/S2/S1}$, and ClC-3c by measuring the area under the off-gating (Q_{off}) currents and plotting these "gating" charges *versus* the preceding voltage steps (12, 16, 37). This analysis revealed identical voltage dependences with a half-maximal activation voltage of ~+65mV for all ClC-3s proteins (Fig. 5*C*). A plot of gating charge *versus* ionic current at the same voltage revealed identical transport competences for all ClC-3 splice variants expressed in the central nervous system (Fig. 5*D*). We conclude that alternative splicing leaves functional properties of ClC-3 unaffected.

ClC-3c Localizes to Recycling Endosomes—Upon heterologous expression in cultured cells, ClC-3c was targeted to different subcellular organelles than ClC-3a or ClC-3b. ClC-3a and 3b show extensive co-localization with the late endosomal/lysosomal markers RAB7/LAMP1, but not with the recycling endosomal marker RAB11 (38, 39) (Figs. 3*B* and 6, *A* and *B*). In contrast, ClC-3c displays a perinuclear distribution with a significant fraction of the protein being located at the plasma membrane. Co-localization with RAB11 (Fig. 6*C*), together

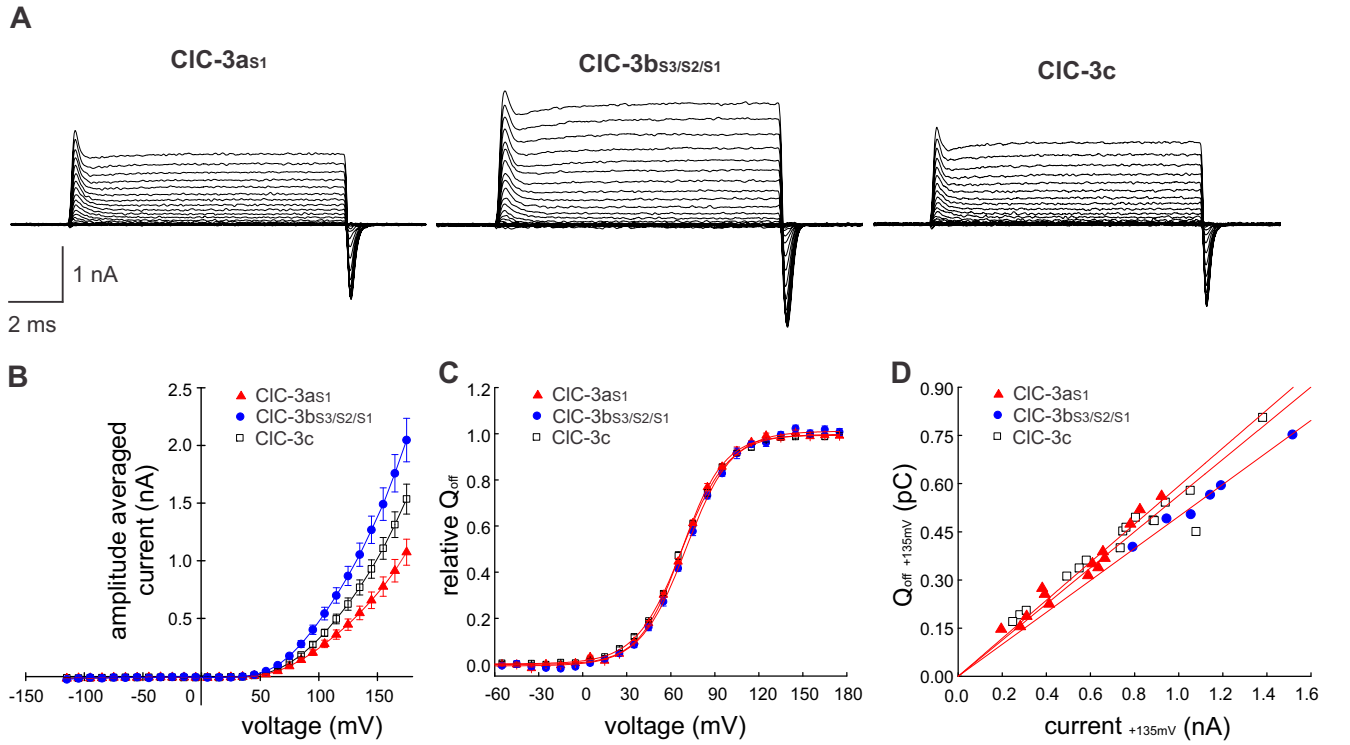

FIGURE 5. **Alternative splicing of *Clcn3* leaves functional properties unaffected.** *A,* representative whole-cell recording from cell expressing ClC-$3a_{S1}$, ClC-$3b_{S3/S2/S1}$, or ClC-3c. *B,* voltage dependence of mean current amplitudes. *C,* voltage dependence of the gating charge movements (Q_{off}). Lines represent nonlinear fits to the data with standard Boltzmann function. *D,* plot of gating charges *versus* ionic current at the same voltage (+135 mV). Lines represent linear fits with zero origin to the data from cells expressing ClC-$3a_{S1}$ ($n = 14$), ClC-$3b_{S3/S2/S1}$ ($n = 7$), or ClC-3c ($n = 20$).

with the limited overlap with LAMP1 or RAB7 (Figs. 3*B* and 6*C*), indicates localization of ClC-3c in the recycling endosome.

Among recycling endosomes two functionally distinct populations can be distinguished: endosomes that express RAB11 (38) and endosomes that contain the transferrin receptor TfR (40). To further study the localization of ClC-3c we co-expressed ClC-3c-eGFP with the transferrin receptor TfR. We observed substantial co-localization ClC-3c with TfR (Fig. 6*C*) indicating that ClC-3c localizes to both, RAB11- and TfR-positive compartments.

ClC-3c Targets to Recycling Endosomes via an Isoleucine-Proline (IP) Motif—ClC-3a, ClC-3b, and ClC-3c share dileucine motifs in the N terminus, and the distinct subcellular localization of ClC-3c must therefore be caused by additional targeting sequences. The ClC-3c N terminus contains a sequence motif (^{8}YLPY^{11}), which is reminiscent of a consensus binding motif Y*XX*[FYL] for AP1, AP2, AP3, and AP4 mu subunits (41, 42). This motif contains the PY residues that were suggested to result in the internalization of ClC-5 and barttin (43, 44) (Fig. 7*A*). To determine whether ^{8}YLPY^{11} is involved in ClC-3c targeting, we substituted all amino acids by alanine and evaluated whether removal of this motif redirects ClC-3c from recycling endosomes to late endosomes/lysosomes. Such a change in localization would be visible as co-localization of mutant ClC-3c with the late endosomal/lysosomal markers RAB7/LAMP1 and characteristic enlargement of endosomal/lysosomal vesicles in cells expressing mutant ClC-3c. However, mutation of all amino acids in ^{8}YLPY^{11} to alanine neither resulted in obvious changes in the subcellular distribution nor in the morphology of intracellular compartments (data not shown).

We next progressively deleted the N-terminal region of ClC-3c by removing stretches of 5, 6, or 8 amino acids (Fig. 7*A*). Neither deletion of the first five amino acids (ClC-$3c_{\Delta 1-5}$, data not shown) nor of the following six amino acids (ClC-$3c_{\Delta 6-11}$) (Fig. 7*B*) changed the localization of the protein or the morphology of intra-vesicular compartments. In contrast, the subsequent deletion of the amino acids stretch ^{12}DGGGDSIP^{19} caused insertion of ClC-$3c_{\Delta 12-19}$ into lysosomes and enlargement of endosomal vesicles (Fig. 7*C*). We observed substantial co-localization of ClC-$3c_{\Delta 12-19}$ with LAMP1, but not with Rab11. Further deletion ClC-$3c_{\Delta 20-25}$ did not alter the subcellular distribution (data not shown). Fusing DGGGDSIP directly to the N terminus of ClC-3a (Fig. 8*A*) resulted in localization of ClC-$3a_{DGGGDSIP}$ in the recycling endosomes (Fig. 8*B*). This result was confirmed by different co-localization pattern of RAB11/LAMP1 with ClC-3a or ClC-$3a_{DGGGDSIP}$ and by the absence of large vesicles formation in cells expressing ClC-$3a_{DGGGDSIP}$ (Fig. 8*B*). Taken together, our findings indicate that the amino acids stretch ^{12}DGGGDSIP^{19} contains a potential sorting motif to the recycling endosome.

To delineate the minimum sequence necessary for the specific sorting of ClC-3c, we mutated groups of two amino acids within this stretch jointly to alanine. Substitution of Asp^{12} and Asp^{16} to alanine (ClC-$3c_{D12/A\ D16/A}$) left targeting of ClC-3c unaltered (Fig. 8, *A* and *C*). In contrast, alanine insertion at ^{18}I and ^{19}P (ClC-$3c_{IP/AA}$) was sufficient to target mutant ClC-3c to late endosomes/lysosomes (Fig. 8, *A* and *D*), resulting in prom-

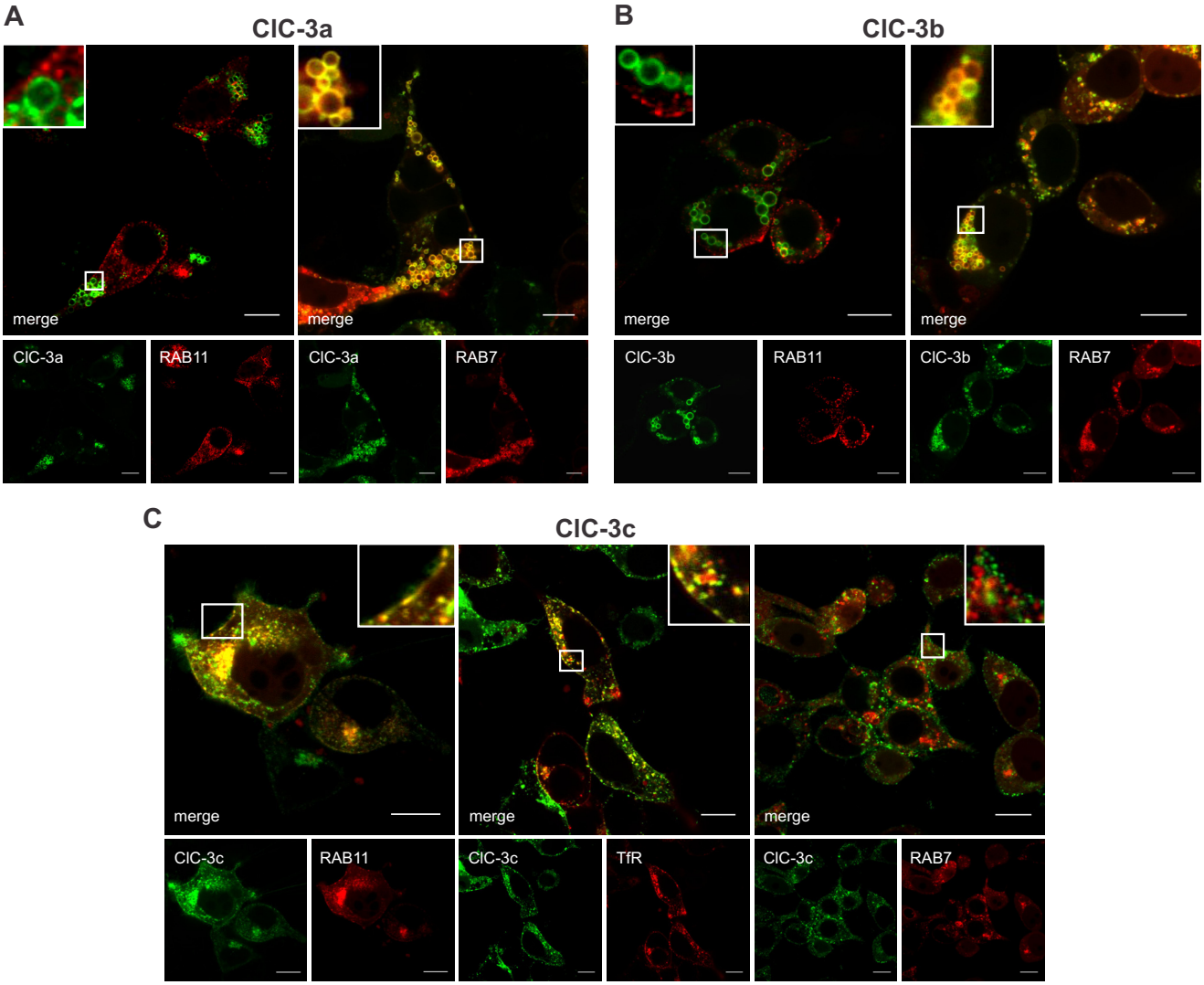

FIGURE 6. **Subcellular localization of ClC-3 splices variants.** *A, B,* confocal images of cells co-transfected with ClC-3a (*A*) or ClC-3b (*B*) and the recycling endosomal marker RAB11 or the late endosomal marker RAB7. *C,* confocal images of cells co-expressing ClC-3c either with RAB11, TfR or RAB7. The scale bar represents 10 μm. *Insets* show the enlargement of vesicular structures upon expression of ClC-3a or ClC-3b, but not of ClC-3c.

inent vesicular enlargement of LAMP1 positive compartments in cells expressing mutant ClC-3c. We conclude that an N-terminal isoleucine-proline (IP) motif is responsible for targeting of ClC-3c to the recycling endosomes.

Discussion

Alternative splicing permits translation of diverse proteins from a single gene by including or excluding certain exons from the processed messenger RNA. We here studied alternative splicing of *Clcn3* and the consequences of this process on protein function and subcellular distribution. The exon-intron arrangement of *Clcn3* suggests translation of six alternatively spliced gene products, referred to as ClC-3a to ClC-3f. We amplified ClC-3 splice variant from different mouse tissues by RT-PCR (Fig. 1*A*) and demonstrated that only three splice variants are expressed in the brain, the olfactory bulb and the spinal cord, ClC-3a, ClC-3b, and ClC-3c, with ClC-3b and ClC-3c being the predominant ClC-3 splice variants (Fig. 1*C* and Fig. 2).

Upon heterologous expression in mammalian cells ClC-3a and ClC-3b exclusively localize to the late endosomal/lysosomal system, whereas ClC-3c can be found in recycling endosomes and also in the surface plasma membrane. ClC-3b is targeted to the late endosomal/lysosomal system via multiple dileucine retention signals (Fig. 4, *A* and *B*), similar to the signals that control localization of ClC-3a (8, 16). For ClC-3c we identified an isoleucine-proline (IP) signal that is responsible for recycling endosome localization. Removal of this signal hinders targeting to recycling endosomes and surface membrane expression of ClC-3c (Fig. 8). Moreover, insertion of the isoleucine-proline (IP) signals reroutes ClC-3a from the late endosomal/lysosomal system to the recycling endosomes (Fig. 8).

We studied localization of ClC-3 splice variants exclusively in cultured mammalian cells of epithelial origin and not in cultured neurons or even native neuronal tissue. Cultured cells are well established for studying trafficking and function of membrane transport proteins, and a large body of evidence supports the notion that similar motifs might direct targeting in epithelia

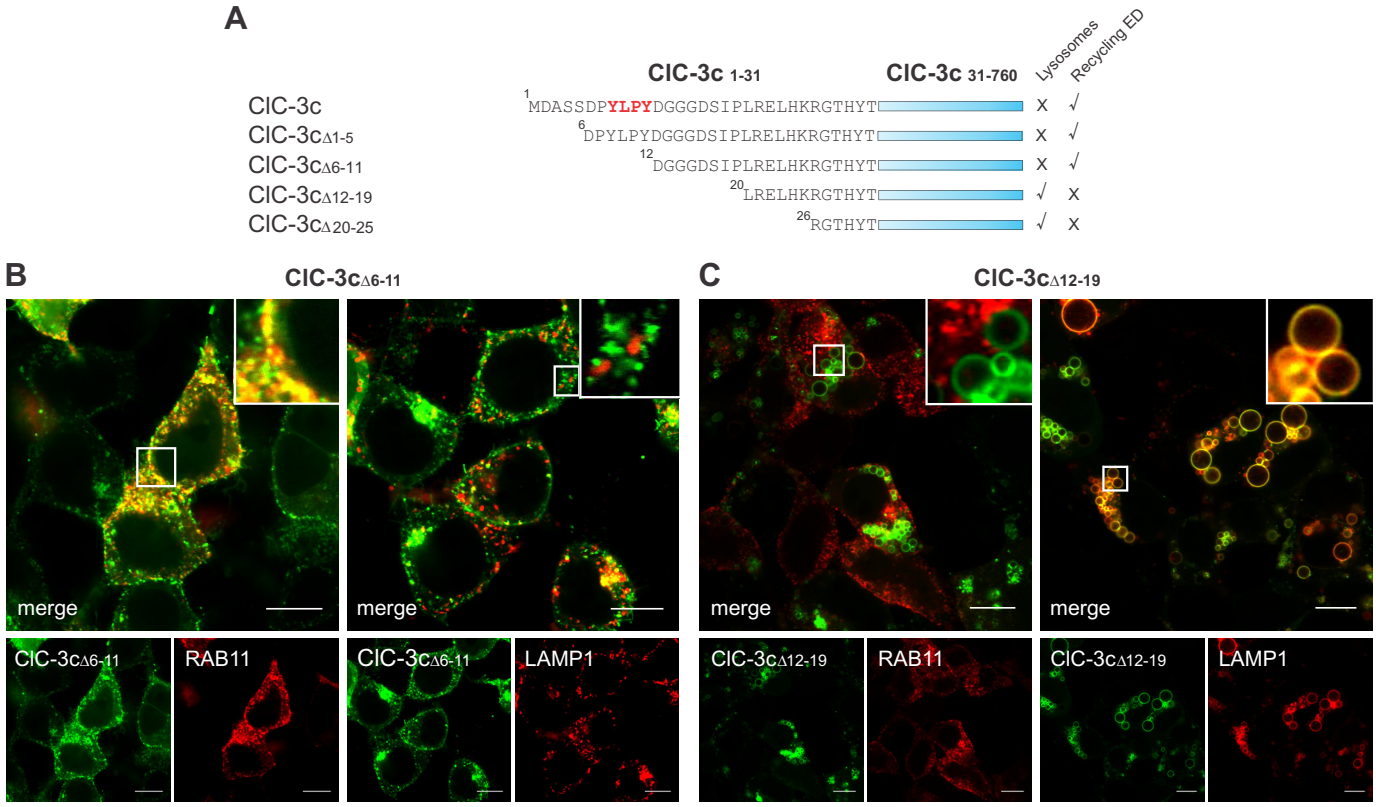

FIGURE 7. **The amino acid stretch ^{12}DGGGDSIP^{19} contains the sorting signal of ClC-3c to recycling endosomes.** *A,* schematic representation of the strategy used to identify the amino acid stretch that contains the ClC-3c targeting signal. *B, C,* confocal images of HEK293T cells co-expressing the N-terminal deletion mutants ClC-3c$_{\Delta 6-11}$ (*B*) or ClC-3c$_{\Delta 12-19}$ (*C*) with RAB11 or LAMP1. *Bars* represent 10 μm. Insets illustrate changes in cell morphology upon expression with ClC-3c$_{\Delta 12-19}$, demonstrating protein localization in the late endosomal/lysosomal system.

and neurons (45). However, there are examples of different subcellular targeting of certain proteins in HEK293T cells and in neurons (46). Thus, although our work conclusively demonstrates separate subcellular localizations of ClC-3a, ClC-3b, and ClC-3c, it does not allow conclusions about which organelles ClC-3 splice variants insert into native neurons.

Recently, the ClC-3 splice variant ClC-3d was cloned from mouse liver and functionally analyzed by heterologous expression in HEK293T cells (20). The authors demonstrated that ClC-3d differed from ClC-3a and ClC-3b in surface membrane expression, but exhibit similar transport properties. These results demonstrate that alternative splicing within the C terminus also affects only trafficking and not function of ClC-3.

All three ClC-3 splice variants in the mammalian central nervous systems exhibit closely similar transport properties. We recently performed a detailed electrophysiological analysis of ClC-3a and demonstrated that this splice variant functions as Cl^--H^+ exchanger with low transport efficiency (16). ClC-3a, ClC-3b, and ClC-3c exhibit identical ratios of the moved charges by the transport current (providing values proportional to the number of complete transport cycles (Fig. 5*D*)) and identical voltage dependences of these capacitive currents (Fig. 5*C*). The importance of these specific functional features of ClC-3 is not clear (16). The extreme outward rectification results in maximum transport rates at voltages far away from physiological values. The large percentage of incomplete transport cycles result in transport effectivities that are much lower than those of ClC-4 and ClC-5 (16). To account for the multiple pronounced effects of ClC-3 ablation we recently proposed that the main function of ClC-3 might be enlarging the capacitance of their resident compartments (16). Such a function nicely accounts for the effects of ClC-3 ablation for synaptic function, but makes it difficult to assign a cellular role for ClC-3 splice variants in early or late endosomes/lysosomes.

Because of its predominant intracellular localization, the functional characterization of ClC-3 has been difficult and multiple transport functions have been assigned to ClC-3 since its identification. Initially, a large conductance, slightly outwardly rectifying anion channel, which was blocked by intracellular calcium, was assigned to ClC-3 (47, 48). Later, ClC-3 was postulated to represent a volume-activated anion channel (49–52). Another ClC-3 candidate channel is a Ca^{2+}/calmodulin-dependent chloride channel at postsynaptic localizations (10, 17). Work with *Clcn3*$^{-/-}$ mice (2) and our functional data on all existing ClC-3 splice variants strongly suggests that these anion channels are not identical with ClC-3 and demonstrate that neuronal ClC-3 splice variants rather function as Cl^--H^+ exchangers with strong voltage dependence and low transport efficiency.

ClC-3a and ClC-3b localize to the late endosomal/lysosomal system and thus partially overlap with the expression pattern of ClC-6 and ClC-7. ClC-6 localizes to the late endosome (53–55), and ClC-7 is a major anion transport protein in lysosomes (56). Since ClC-3 (16), ClC-6 (46), and ClC-7 (57) are all chloride-proton exchangers, one might expect that these overlapping localizations permit compensatory mechanisms upon genetic

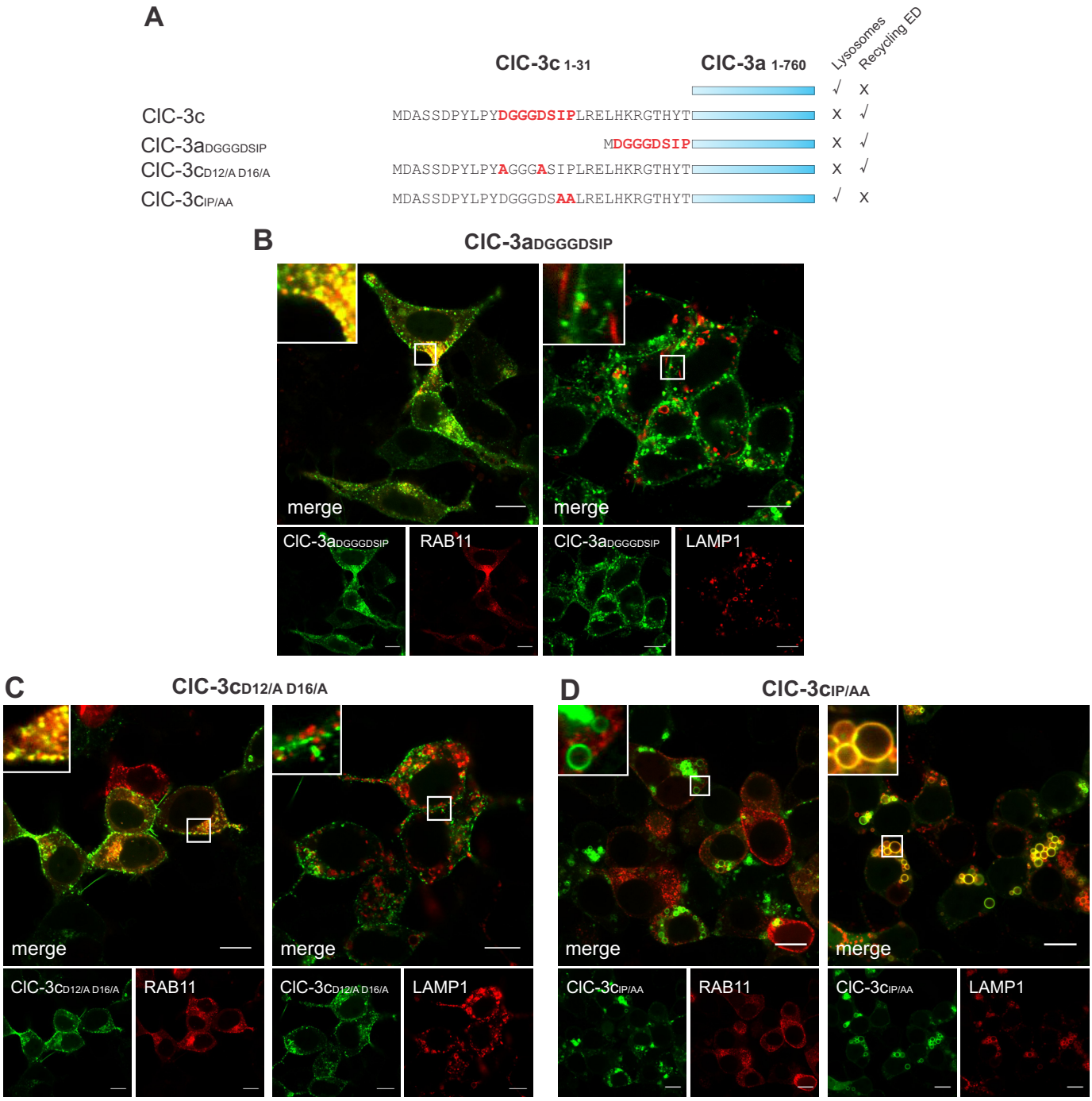

FIGURE 8. **ClC-3c is targeted to recycling endosomes via an IP motif.** *A*, schematic representation of the approach used to dissect the sorting signal of ClC-3c. Amino acid substitutions and insertions are highlighted in red. *B*, *C*, *D*, confocal images of HEK293T cells co-expressing ClC-3a$_{DGGGDSIP}$ (*B*), ClC-3c$_{D12/A\ D16/A}$ (*C*) or ClC-3c$_{IP/AA}$ (*D*) with RAB11 or LAMP1. The scale bar represents 10 μm. *Insets* show changes in cell morphology upon expression of ClC-3c$_{IP/AA}$, but neither with ClC-3a$_{DGGGDSIP}$ nor with ClC-3c$_{D12/A\ D16/A}$.

removal of one of these isoforms. However, the severe phenotypes of animals, in which only one of these three transporters is genetically removed (1–3, 53, 54), demonstrates that this is not the case.

Whereas ClC-3a and ClC-3b can only be found in intracellular compartments, ClC-3c is part of the recycling endosome with a considerable percentage of transporters present in the surface membrane. ClC-3c co-localizes with endosomes that express RAB11 as well as with endosomes that contain the transferrin receptor TfR (31). RAB11 is present in mature synaptic vesicles of the mammalian brain, and it has been speculated that it might contribute in determining the secretory fate of a transport vesicle (58). Upon expression in cultured neurons, RAB11 localizes to synaptic boutons and moderately co-purifies with synaptic vesicle markers (59). So far, we have not determined the localization of the different splice variants in neurons, but these data suggest that ClC-3c might account for altered synaptic transmission in *Clcn3*$^{-/-}$ (2, 4, 5). Alternative

splicing of ClC-3 permits targeting intracellular CLC transporters to multiple distinct cellular compartments. ClC-3 is known to hetero-multimerize with ClC-4 and ClC-5 (60), and alternative splicing of ClC-3 will thus also affect subcellular localization of ClC-3-ClC-4 oligomers in the central nervous system. Moreover, hetero-dimers between different splice variants are likely to assemble. At present, it is not clear into which compartment these different hetero-oligomers will insert.

In summary, we demonstrate that alternative splicing leads to the occurrence of three ClC-3 splice variant with differences in the N terminus in the mammalian system. All three variants exhibit identical transport properties, but distinct localization in late endosomes/lysosomes or recycling endosomes. Alternative splicing enables ClC-3 to fulfill diverse cellular functions, and our work provides an important step toward understanding the role of ClC-3 in diverse cellular compartments.

Author Contributions—R. E. G. planned, performed, and analyzed experiments and wrote the manuscript. E. M. L. planned, performed, and analyzed experiments. A. F. planned and performed experiments. Ch. F. planned experiments and wrote the manuscript.

Acknowledgments—We thank Drs. Arnd Baumann, Cora Hannack, Patricia Hidalgo, and Gabriel Stölting for helpful discussions, and Joachim Schmitz and Petra Thelen for excellent technical assistance.

References

1. Dickerson, L. W., Bonthius, D. J., Schutte, B. C., Yang, B., Barna, T. J., Bailey, M. C., Nehrke, K., Williamson, R. A., and Lamb, F. S. (2002) Altered GABAergic function accompanies hippocampal degeneration in mice lacking ClC-3 voltage-gated chloride channels. *Brain Res.* **958,** 227–250
2. Stobrawa, S. M., Breiderhoff, T., Takamori, S., Engel, D., Schweizer, M., Zdebik, A. A., Bösl, M. R., Ruether, K., Jahn, H., Draguhn, A., Jahn, R., and Jentsch, T. J. (2001) Disruption of ClC-3, a chloride channel expressed on synaptic vesicles, leads to a loss of the hippocampus. *Neuron* **29,** 185–196
3. Yoshikawa, M., Uchida, S., Ezaki, J., Rai, T., Hayama, A., Kobayashi, K., Kida, Y., Noda, M., Koike, M., Uchiyama, Y., Marumo, F., Kominami, E., and Sasaki, S. (2002) CLC-3 deficiency leads to phenotypes similar to human neuronal ceroid lipofuscinosis. *Genes Cells* **7,** 597–605
4. Guzman, R. E., Alekov, A. K., Filippov, M., Hegermann, J., and Fahlke, Ch. (2014) Involvement of ClC-3 chloride/proton exchangers in controlling glutamatergic synaptic strength in cultured hippocampal neurons. *Front Cell Neurosci.* **8,** 143
5. Riazanski, V., Deriy, L. V., Shevchenko, P. D., Le, B., Gomez, E. A., and Nelson, D. J. (2011) Presynaptic CLC-3 determines quantal size of inhibitory transmission in the hippocampus. *Nat. Neurosci.* **14,** 487–494
6. Li, X., Wang, T., Zhao, Z., and Weinman, S. A. (2002) The ClC-3 chloride channel promotes acidification of lysosomes in CHO-K1 and Huh-7 cells. *Am. J. Physiol. Cell Physiol.* **282,** C1483-C1491
7. Maritzen, T., Keating, D. J., Neagoe, I., Zdebik, A. A., and Jentsch, T. J. (2008) Role of the vesicular chloride transporter ClC-3 in neuroendocrine tissue. *J. Neurosci.* **28,** 10587–10598
8. Zhao, Z., Li, X., Hao, J., Winston, J. H., and Weinman, S. A. (2007) The ClC-3 chloride transport protein traffics through the plasma membrane via interaction of an N-terminal dileucine cluster with clathrin. *J. Biol. Chem.* **282,** 29022–29031
9. Farmer, L. M., Le, B. N., and Nelson, D. J. (2013) CLC-3 chloride channels moderate long-term potentiation at Schaffer collateral-CA1 synapses. *J. Physiol.* **591,** 1001–1015
10. Wang, X. Q., Deriy, L. V., Foss, S., Huang, P., Lamb, F. S., Kaetzel, M. A., Bindokas, V., Marks, J. D., and Nelson, D. J. (2006) CLC-3 channels modulate excitatory synaptic transmission in hippocampal neurons. *Neuron* **52,** 321–333
11. Alekov, A. K., and Fahlke, Ch. (2009) Channel-like slippage modes in the human anion/proton exchanger ClC-4. *J. Gen. Physiol.* **133,** 485–496
12. Grieschat, M., and Alekov, A. K. (2012) Glutamate 268 regulates transport probability of the anion/proton exchanger ClC-5. *J. Biol. Chem.* **287,** 8101–8109
13. Orhan, G., Fahlke, Ch., and Alekov, A. K. (2011) Anion- and proton-dependent gating of ClC-4 anion/proton transporter under uncoupling conditions. *Biophys. J.* **100,** 1233–1241
14. Picollo, A., and Pusch, M. (2005) Chloride/proton antiporter activity of mammalian CLC proteins ClC-4 and ClC-5. *Nature* **436,** 420–423
15. Scheel, O., Zdebik, A. A., Lourdel, S., and Jentsch, T. J. (2005) Voltage-dependent electrogenic chloride/proton exchange by endosomal CLC proteins. *Nature* **436,** 424–427
16. Guzman, R. E., Grieschat, M., Fahlke, Ch., and Alekov, A. K. (2013) ClC-3 is an intracellular chloride/proton exchanger with large voltage-dependent nonlinear capacitance. *ACS Chem. Neurosci.* **4,** 994–1003
17. Huang, P., Liu, J., Di, A., Robinson, N. C., Musch, M. W., Kaetzel, M. A., and Nelson, D. J. (2001) Regulation of human CLC-3 channels by multifunctional Ca^{2+}/calmodulin-dependent protein kinase. *J. Biol. Chem.* **276,** 20093–20100
18. Gentzsch, M., Cui, L., Mengos, A., Chang, X. B., Chen, J. H., and Riordan, J. R. (2003) The PDZ-binding chloride channel ClC-3B localizes to the Golgi and associates with cystic fibrosis transmembrane conductance regulator-interacting PDZ proteins. *J. Biol. Chem.* **278,** 6440–6449
19. Ogura, T., Furukawa, T., Toyozaki, T., Yamada, K., Zheng, Y. J., Katayama, Y., Nakaya, H., and Inagaki, N. (2002) ClC-3B, a novel ClC-3 splicing variant that interacts with EBP50 and facilitates expression of CFTR-regulated ORCC. *FASEB J.* **16,** 863–865
20. Okada, T., Akita, T., Sato-Numata, K., Islam, M. R., and Okada, Y. (2014) A newly cloned ClC-3 isoform, ClC-3d, as well as ClC-3a mediates Cd-sensitive outwardly rectifying anion currents. *Cell Physiol. Biochem.* **33,** 539–556
21. Schneider, C. A., Rasband, W. S., and Eliceiri, K. W. (2012) NIH Image to ImageJ: 25 years of image analysis. *Nat. Methods* **9,** 671–675
22. Sherer, N. M., Lehmann, M. J., Jimenez-Soto, L. F., Ingmundson, A., Horner, S. M., Cicchetti, G., Allen, P. G., Pypaert, M., Cunningham, J. M., and Mothes, W. (2003) Visualization of retroviral replication in living cells reveals budding into multivesicular bodies. *Traffic* **4,** 785–801
23. Choudhury, A., Dominguez, M., Puri, V., Sharma, D. K., Narita, K., Wheatley, C. L., Marks, D. L., and Pagano, R. E. (2002) Rab proteins mediate Golgi transport of caveola-internalized glycosphingolipids and correct lipid trafficking in Niemann-Pick C cells. *J. Clin. Invest.* **109,** 1541–1550
24. Burack, M. A., Silverman, M. A., and Banker, G. (2000) The role of selective transport in neuronal protein sorting. *Neuron* **26,** 465–472
25. Fahlke, Ch., Desai, R. R., Gillani, N., and George, A. L., Jr. (2001) Residues lining the inner pore vestibule of human muscle chloride channels. *J. Biol. Chem.* **276,** 1759–1765
26. Bezanilla, F., and Armstrong, C. M. (1977) Inactivation of the sodium channel. I. Sodium current experiments. *J. Gen. Physiol.* **70,** 549–566
27. Hidalgo, P., Gonzalez-Gutierrez, G., Garcia-Olivares, J., and Neely, A. (2006) The alpha1-beta-subunit interaction that modulates calcium channel activity is reversible and requires a competent alpha-interaction domain. *J. Biol. Chem.* **281,** 24104–24110
28. Miranda-Laferte, E., Ewers, D., Guzman, R. E., Jordan, N., Schmidt, S., and Hidalgo, P. (2014) The N-terminal domain tethers the voltage-gated calcium channel β2e-subunit to the plasma membrane via electrostatic and hydrophobic interactions. *J. Biol. Chem.* **289,** 10387–10398
29. Smith, A. J., and Lippiat, J. D. (2010) Voltage-dependent charge movement associated with activation of the CLC-5 $2Cl^-/1H^+$ exchanger. *FASEB J.* **24,** 3696–3705
30. Ferrera, L., Caputo, A., Ubby, I., Bussani, E., Zegarra-Moran, O., Ravazzolo, R., Pagani, F., and Galietta, L. J. (2009) Regulation of TMEM16A chloride channel properties by alternative splicing. *J. Biol. Chem.* **284,** 33360–33368
31. Stocker, M., Stühmer, W., Wittka, R., Wang, X., Müller, R., Ferrus, A., and Pongs, O. (1990) Alternative *Shaker* transcripts express either rapidly inactivating or noninactivating K^+ channels. *Proc. Natl. Acad. Sci. U.S.A.* **87,**

8903–8907
32. Suzuki, T., Suzuki, J., and Nagata, S. (2014) Functional swapping between transmembrane proteins TMEM16A and TMEM16F. *J. Biol. Chem.* **289,** 7438–7447
33. Timpe, L. C., Jan, Y. N., and Jan, L. Y. (1988) Four cDNA clones from the Shaker locus of Drosophila induce kinetically distinct A-type potassium currents in Xenopus oocytes. *Neuron* **1,** 659–667
34. Stauber, T., and Jentsch, T. J. (2010) Sorting motifs of the endosomal/lysosomal CLC chloride transporters. *J. Biol. Chem.* **285,** 34537–34548
35. Gough, N. R., Zweifel, M. E., Martinez-Augustin, O., Aguilar, R. C., Bonifacino, J. S., and Fambrough, D. M. (1999) Utilization of the indirect lysosome targeting pathway by lysosome-associated membrane proteins (LAMPs) is influenced largely by the C-terminal residue of their GYXXϕ targeting signals. *J. Cell Sci.* **112,** 4257–4269
36. Zifarelli, G., De Stefano, S., Zanardi, I., and Pusch, M. (2012) On the mechanism of gating charge movement of ClC-5, a human Cl^-/H^+ antiporter. *Biophys. J.* **102,** 2060–2069
37. Grieschat, M., and Alekov, A. K. (2014) Multiple discrete transitions underlie voltage-dependent activation in CLC Cl^-/H^+ antiporters. *Biophys. J.* **107,** L13–15
38. Kobayashi, H., and Fukuda, M. (2013) Arf6, Rab11 and transferrin receptor define distinct populations of recycling endosomes. *Commun Integr Biol.* **6,** e25036
39. Ullrich, O., Reinsch, S., Urbé, S., Zerial, M., and Parton, R. G. (1996) Rab11 regulates recycling through the pericentriolar recycling endosome. *J. Cell Biol.* **135,** 913–924
40. Maxfield, F. R., and McGraw, T. E. (2004) Endocytic recycling. *Nat. Rev. Mol. Cell Biol.* **5,** 121–132
41. Bonifacino, J. S., and Traub, L. M. (2003) Signals for sorting of transmembrane proteins to endosomes and lysosomes. *Ann. Rev. Biochem.* **72,** 395–447
42. Collawn, J. F., Stangel, M., Kuhn, L. A., Esekogwu, V., Jing, S. Q., Trowbridge, I. S., and Tainer, J. A. (1990) Transferrin receptor internalization sequence YXRF implicates a tight turn as the structural recognition motif for endocytosis. *Cell* **63,** 1061–1072
43. Estévez, R., Boettger, T., Stein, V., Birkenhäger, R., Otto, E., Hildebrandt, F., and Jentsch, T. J. (2001) Barttin is a Cl^- channel beta-subunit crucial for renal Cl^- reabsorption and inner ear K^+ secretion. *Nature* **414,** 558–561
44. Schwake, M., Friedrich, T., and Jentsch, T. J. (2001) An internalization signal in ClC-5, an endosomal Cl^- channel mutated in dent's disease. *J. Biol. Chem.* **276,** 12049–12054
45. Cheng, C., Glover, G., Banker, G., and Amara, S. G. (2002) A novel sorting motif in the glutamate transporter excitatory amino acid transporter 3 directs its targeting in Madin-Darby canine kidney cells and hippocampal neurons. *J. Neurosci.* **22,** 10643–10652
46. Neagoe, I., Stauber, T., Fidzinski, P., Bergsdorf, E. Y., and Jentsch, T. J. (2010) The late endosomal ClC-6 mediates proton/chloride countertransport in heterologous plasma membrane expression. *J. Biol. Chem.* **285,** 21689–21697
47. Kawasaki, M., Uchida, S., Monkawa, T., Miyawaki, A., Mikoshiba, K., Marumo, F., and Sasaki, S. (1994) Cloning and expression of a protein kinase C-regulated chloride channel abundantly expressed in rat brain neuronal cells. *Neuron.* **12,** 597–604
48. Kawasaki, M., Suzuki, M., Uchida, S., Sasaki, S., and Marumo, F. (1995) Stable and functional expression of the CIC-3 chloride channel in somatic cell lines. *Neuron.* **14,** 1285–1291
49. Duan, D., Winter, C., Cowley, S., Hume, J. R., and Horowitz, B. (1997) Molecular identification of a volume-regulated chloride channel. *Nature* **390,** 417–421
50. Yamazaki, J., Duan, D., Janiak, R., Kuenzli, K., Horowitz, B., and Hume, J. R. (1998) Functional and molecular expression of volume-regulated chloride channels in canine vascular smooth muscle cells. *J. Physiol.* **507,** 729–736
51. Mao, J., Chen, L., Xu, B., Wang, L., Wang, W., Li, M., Zheng, M., Li, H., Guo, J., Li, W., Jacob, T. J., and Wang, L. (2009) Volume-activated chloride channels contribute to cell-cycle-dependent regulation of HeLa cell migration. *Biochem. Pharmacol.* **77,** 159–168
52. Zhang, H., Li, H., Liu, E., Guang, Y., Yang, L., Mao, J., Zhu, L., Chen, L., and Wang, L. (2014) The AQP-3 water channel and the ClC-3 chloride channel coordinate the hypotonicity-induced swelling volume in nasopharyngeal carcinoma cells. *Int. J. Biochem. Cell Biol.* **57,** 96–107
53. Poët, M., Kornak, U., Schweizer, M., Zdebik, A. A., Scheel, O., Hoelter, S., Wurst, W., Schmitt, A., Fuhrmann, J. C., Planells-Cases, R., Mole, S. E., Hübner, C. A., and Jentsch, T. J. (2006) Lysosomal storage disease upon disruption of the neuronal chloride transport protein ClC-6. *Proc. Natl. Acad. Sci. U.S.A.* **103,** 13854–13859
54. Kornak, U., Kasper, D., Bösl, M. R., Kaiser, E., Schweizer, M., Schulz, A., Friedrich, W., Delling, G., and Jentsch, T. J. (2001) Loss of the ClC-7 chloride channel leads to osteopetrosis in mice and man. *Cell* **104,** 205–215
55. Weinert, S., Jabs, S., Supanchart, C., Schweizer, M., Gimber, N., Richter, M., Rademann, J., Stauber, T., Kornak, U., and Jentsch, T. J. (2010) Lysosomal pathology and osteopetrosis upon loss of H^+-driven lysosomal Cl^- accumulation. *Science* **328,** 1401–1403
56. Graves, A. R., Curran, P. K., Smith, C. L., and Mindell, J. A. (2008) The Cl^-/H^+ antiporter ClC-7 is the primary chloride permeation pathway in lysosomes. *Nature* **453,** 788–792
57. Leisle, L., Ludwig, C. F., Wagner, F. A., Jentsch, T. J., and Stauber, T. (2011) ClC-7 is a slowly voltage-gated $2Cl^-/1H^+$-exchanger and requires Ostm1 for transport activity. *EMBO J.* **30,** 2140–2152
58. Khvotchev, M. V., Ren, M., Takamori, S., Jahn, R., and Südhof, T. C. (2003) Divergent functions of neuronal Rab11b in Ca^{2+}-regulated versus constitutive exocytosis. *J. Neurosci.* **23,** 10531–10539
59. Pavlos, N. J., Grønborg, M., Riedel, D., Chua, J. J., Boyken, J., Kloepper, T. H., Urlaub, H., Rizzoli, S. O., and Jahn, R. (2010) Quantitative analysis of synaptic vesicle Rabs uncovers distinct yet overlapping roles for Rab3a and Rab27b in Ca^{2+}-triggered exocytosis. *J. Neurosci.* **30,** 13441–13453
60. Suzuki, T., Rai, T., Hayama, A., Sohara, E., Suda, S., Itoh, T., Sasaki, S., and Uchida, S. (2006) Intracellular localization of ClC chloride channels and their ability to form hetero-oligomers. *J. Cell Physiol.* **206,** 792–798